INFECTION AND IMMUNITY, Oct. 2004, p. 5963–5971 Vol. 72, No. 10
0019-9567/04/$08.00+0 DOI: 10.1128/IAI.72.10.5963–5971.2004

Magnetic Resonance Imaging of Pulmonary Lesions in Guinea Pigs Infected with *Mycobacterium tuberculosis*

Susan L. Kraft,[1] Deanna Dailey,[1] Matthew Kovach,[1] Karen L. Stasiak,[2] Jamie Bennett,[2] Christine T. McFarland,[3] David N. McMurray,[3] Angelo A. Izzo,[2] Ian M. Orme,[2] and Randall J. Basaraba[2]*

Departments of Environmental and Radiological Health Sciences[1] and Microbiology, Immunology, and Pathology,[2] Colorado State University, Fort Collins, Colorado, and Department of Medical Microbiology and Immunology, Texas A&M University, College Station, Texas[3]

Received 1 March 2004/Returned for modification 10 May 2004/Accepted 21 June 2004

We utilized magnetic resonance imaging to visualize lesions in the lungs of guinea pigs infected by low-dose aerosol exposure to *Mycobacterium tuberculosis*. Lesions were prominent in such images, and colorized three-dimensional reconstructions of images revealed a very uniform distribution in the lungs. Lesion numbers after 1 month were approximately similar to the aerosol exposure algorithm, suggesting that each was established by a single bacterium. Numbers of lesions in unprotected and vaccinated animals were similar over the first month but increased thereafter in the control animals, indicating secondary lesion development. Whereas lesion sizes increased progressively in control guinea pigs, lesions remained small in BCG-vaccinated animals. A prominent feature of the disease pathology in unprotected animals was rapid and severe lymphadenopathy of the mediastinal lymph node cluster, which is paradoxical given the strong state of cellular immunity at this time. Further development of this technical approach could be very useful in tracking lesion size, number, and progression in the search for new tuberculosis vaccines.

The ongoing global epidemic of disease caused by infection with *Mycobacterium tuberculosis* continues unabated. In response a significant research effort has been directed toward the development of new vaccine candidates (1, 5, 6, 11, 12, 18, 19). Preclinical screening of these new candidates has mostly been conducted to date in the mouse model, with the most promising of these being evaluated further in the guinea pig model (3, 19).

It is generally agreed that the guinea pig (*Cavia porcellus*) provides a stringent test of new vaccines, given the acute susceptibility of this model to *Mycobacterium tuberculosis* infection and the similarities between the pathology observed in this animal and the disease process in humans (14, 16). A recent comprehensive description of the pathological process in the guinea pig has been provided (25, 26), and this can be used as a framework upon which potentially beneficial effects of new vaccines can be compared.

To date, however, lesion burden in infected guinea pigs has usually been evaluated by gross postmortem examination and histopathology for comparison between treatment groups. Histopathology allows lesion ranking and staging at the cellular level but provides no insight into the total lesion burden. These methods are relatively inexpensive and leave the majority of tissue available for additional procedures (such as determining the lung bacterial load) but have the disadvantage that samples taken may not be representative of the entire lung. Systematic gross sectioning of the entire lung can be done to estimate the number and distribution of pulmonary granulomas, but that is a tedious process and nodules smaller than the slice thickness can still be missed.

Given that the number of established lung lesions and their distribution through the lungs may be a useful indication of a vaccine effect, we have sought new methods to fully visualize the entire lung after aerosol infection with *M. tuberculosis*. We describe here the use of magnetic resonance imaging to evaluate the distribution and total burden of granulomatous lesions in harvested whole-lung samples. The results obtained indicate that lung lesions can be clearly visualized and that application of three-dimensional stacking software can be utilized to give a reconstructed view of the whole lung, allowing an assessment of whole-organ lesion distribution.

MATERIALS AND METHODS

Experimental infections. Female outbred Hartley guinea pigs (~500 g [body weight]) were purchased from the Charles River Laboratories (North Wilmington, Mass.) and held under barrier conditions in a Biosafety Level III animal laboratory. *M. tuberculosis* H37Rv and *M. bovis* BCG Pasteur were grown from low-passage seed lots in Proskauer-Beck liquid medium containing 0.05% Tween 80 to early mid-log phase. Cultures were divided into aliquots into 1-ml tubes and frozen at −70°C until used. Thawed aliquots were diluted in double-distilled sterile water to the desired inoculum concentrations. A Madison chamber aerosol generation device was used to expose the animals to an aerosol of *M. tuberculosis* and was calibrated to deliver ca. 20 bacilli into each guinea pig lung.

Lung fixation. Lungs were harvested from control and vaccinated guinea pigs at various times after exposure to infection with *M. tuberculosis*. At the time of euthanasia, lungs were inflated with ca. 60 ml/kg of room air by tracheal intubation. The pulmonary vasculature was flushed of blood with 45 to 60 ml of phosphate-buffered saline and perfusion fixed with 45 to 60 ml of 10% neutral buffered formalin via the right ventricle. After perfusion fixation, lungs were removed en bloc and immersion fixed overnight in 10% neutral buffered formalin. After overnight fixation, the heart, adjacent vessels, and esophagus of each animal were dissected from the lungs, and the surface was dried. The lungs and associated mediastinal lymph nodes were embedded in 4% low-melting-point agarose in phosphate-buffered saline.

Embedded lungs were sectioned into ca. 18 to 24 2-mm slices by using an

* Corresponding author. Mailing address: Department of Microbiology, Immunology and Pathology, Colorado State University, Fort Collins, CO 80523. Phone: (970) 491-3313. Fax: (970) 491-0603. E-mail: basaraba@colostate.edu.

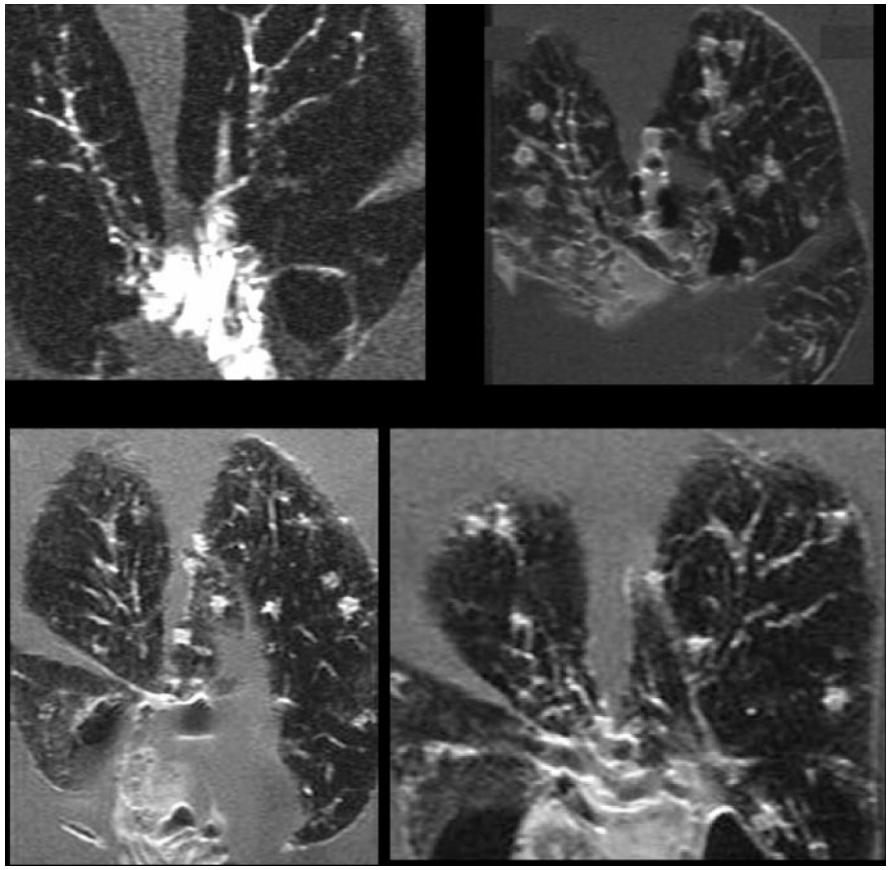

FIG. 1. Magnetic resonance images of lungs of guinea pigs infected by aerosol with *M. tuberculosis*. Lungs were harvested on day 15 of the infection (top left) or on day 30 (other panels).

aluminum template. Furthermore, one section containing a portion of the left caudal lung lobe was taken and processed normally for histological evaluation after being stained with hematoxylin and eosin.

Magnetic resonance imaging. Magnetic resonance imaging was performed at all time points by using a 1.5-T General Electric Medical Systems Signa HiSpeed LX 9.0. Lung images were generated in a standard phased array transmit-receive coil designed for human wrist imaging. The following pulse sequences were used: T1 weighted (TR = 750 ms, TE = 31.0 ms, 512 × 224, FOV 10 cm, 4 NEX), T2 weighted (TR = 6,300.0 ms, TE = 102 to 113.0 ms,512 × 224, FOV 10 cm, 4 NEX), and pathology-weighted STIR (TR = 3,000.0 ms, TE = 40.5 to 50 ms, TI = 150 ms, 256 × 192, 4 NEX). The same slice registration was used for all pulse sequences, with a slice thickness of 1.5 mm and a 0.0-mm space. Thinner slices with T1 weighting were also obtained with a three-dimensional volume sequence (TR = 14.5 ms, TE = 6.7 ms, slice thickness = 0.5 mm, 256 × 192, 3 NEX). All imaging was done in the dorsal plane relative to the lungs. In-plane spatial resolution was 0.2 mm × 0.45 mm with these imaging factors.

Pathological correlation and lesion analysis. Selective histopathological sampling was done based on location of nodules from the images. Lung volumes, total nodular burden, and lymph node volumes were quantitated from the cross-sectional images by using three-dimensional analytical volume software (Voxar, Ltd., Edinburgh, United Kingdom). This software also made possible the rotation of lung reconstructions three dimensionally, allowing assessment of relative relationships of the nodules and normal pulmonary structures through the stages of pathological development.

RESULTS

Magnetic resonance imaging of lesions in vaccinated and unprotected guinea pigs. Images obtained from control guinea pigs are shown in Fig. 1. In animals euthanized 15 days after aerosol exposure (Fig. 1, top left panel), small nodules could be seen in the lung parenchyma and close to the bronchial tree. In animals euthanized after 35 days (other panels), granulomatous lesions were obvious throughout the tissue slices. Many had a ring appearance, a finding consistent with a stronger signal from an outer nodular ring of intact cells, and a lower signal from the center where the tissue has become necrotic (25, 26).

In guinea pigs vaccinated with BCG and then challenged, nodular lesions could be seen in the day 30 post-aerosol-imaging results (Fig. 2). However, these were generally smaller than those in the unprotected animals.

It is normally thought that T2-weighted imaging gives better resolution with fixated tissues. Here, however, T1-weighted imaging had no negative impact because of the tremendous signal differences between the insufflated lung tissue and the tissue granulomas. This provided a great deal of contrast between the air-containing tissue and the lesions despite fixation.

Three-dimensional imaging of whole lungs. Images from each sequential tissue slice were reconstructed and selectively colorized by using computer imaging software, resulting in three-dimensional images of the entire lung. A representative example is given in Fig. 3. This animal was euthanized after 35 days. About 25 to 30 tuberculous lesions (in blue) can be seen; they were similar in size and appear to be uniformly distributed

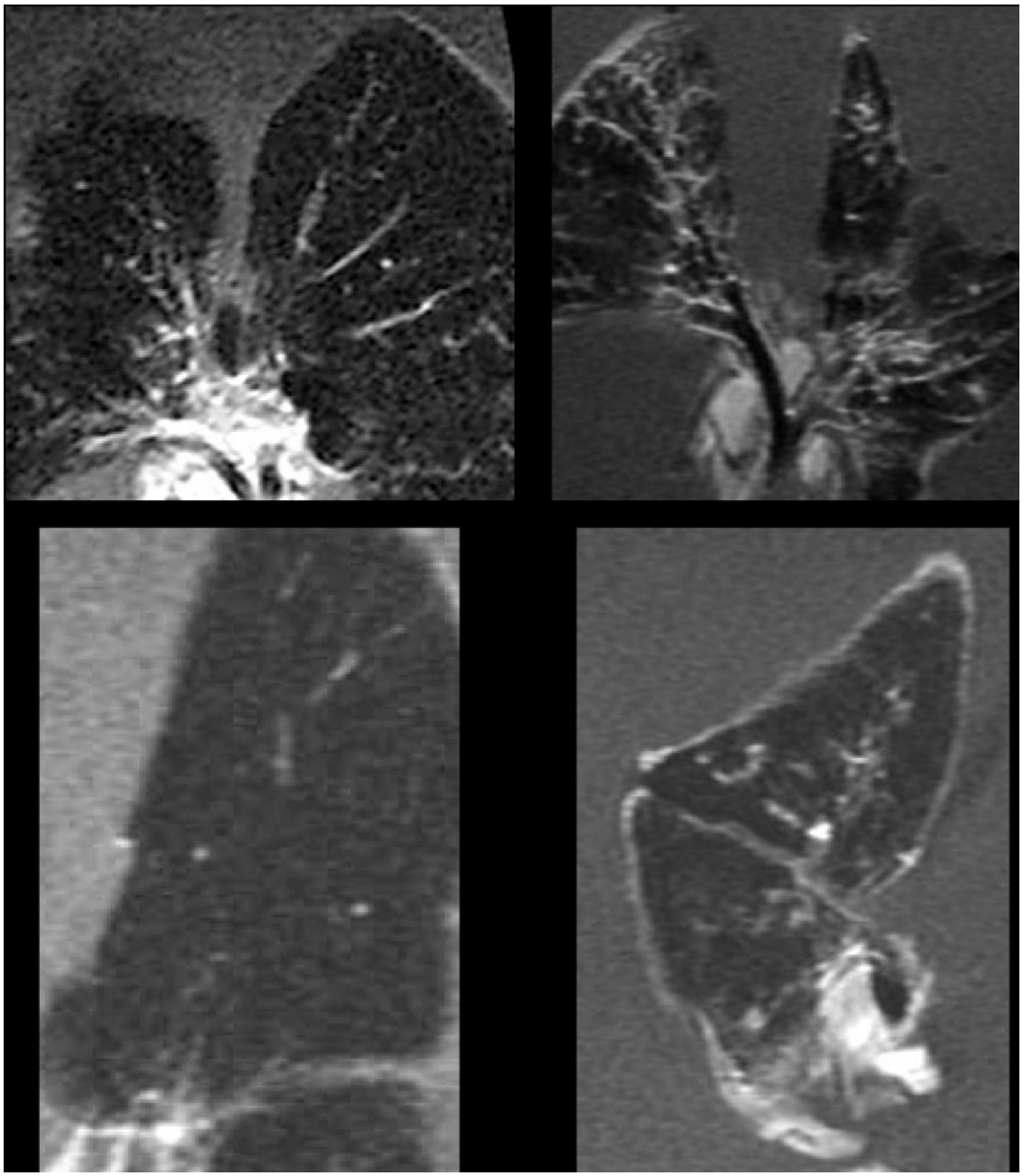

FIG. 2. Magnetic resonance images of lungs of guinea pigs infected by aerosol with *M. tuberculosis* 5 weeks after vaccination with BCG and then harvested and processed 30 days later. Lesions can clearly be seen, but in general they were smaller than in nonvaccinated controls.

across the peribronchial, peribronchiolar, and perivascular areas of the lung. The large gray structure in the figure is the mediastinal lymph node (discussed further below).

A feature of the reconstruction analysis is that it can be rotated in three dimensions. As shown in Fig. 4, this can be used to emphasize the substantial increase in size of the lymph node cluster relative to the animals vaccinated with BCG.

We then used these images to count visible nodules and used the magnetic resonance imaging software to calculate lesion sizes on lungs harvested between days 10 and 50. These data are shown in Fig. 5. It shows, first, that the numbers of lesions in the vaccinated and nonvaccinated animals were similar over the first 30 to 40 days. This increased in the controls thereafter, perhaps indicating the establishment of secondary lesions. Where BCG vaccination had an obvious effect, however, was in the size of the lesions, which remained small in these animals but increased progressively in unprotected animals.

Rapid lymphadenopathy of the mediastinal lymph node in unprotected guinea pigs. Severe lymphadenopathy of the mediastinal lymph node cluster was noticeable throughout these studies, particularly in the control infected guinea pigs by day 30. Figure 6 shows examples of three-dimensional images

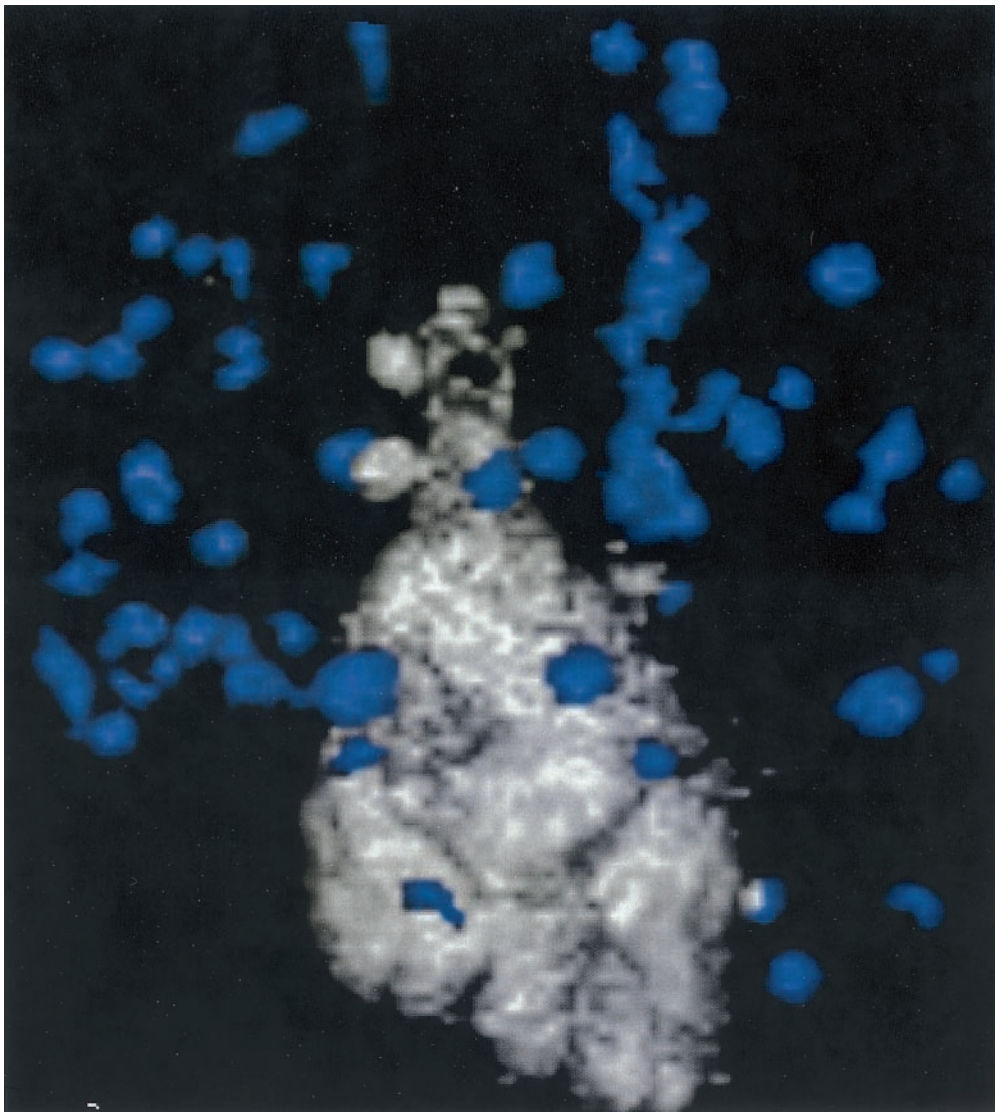

FIG. 3. Three-dimensional colorized reconstruction of a series of magnetic resonance images from a nonvaccinated control guinea pig 30 days after infection by aerosol with *M. tuberculosis*. Granulomatous lesions are blue. The large gray structure is the mediastinal lymph node cluster.

taken from different aspects, illustrating the sheer size of this lymph node cluster, and the very much smaller tissues observed in the BCG-vaccinated animals.

Histopathology of the mediastinal lymph node. Given the above results we also examined the mediastinal lymph node by histology. Figure 7 illustrates the substantial inflammation and damage seen in the nonvaccinated control animals, in which the lymph nodes were markedly enlarged by extensive infiltrates dominated by macrophages and with foci of necrosis that had destroyed much of the cortex and medulla.

DISCUSSION

The results presented here indicate that magnetic resonance technology is a potentially useful new tool for assessing the development of pathology in the lungs of guinea pigs infected with pulmonary tuberculosis. The ability of this type of analysis to provide visual data regarding the distribution of lesions in the lungs, as well as their size and number, may be very useful in new tuberculosis vaccine candidate testing. At this early stage of development the primary limitation appears to be one of sensitivity. As yet, it is hard to be sure that very small nodules are indeed lesions, something that more conventional approaches such as bacteriological culture or microscopy of stained sections can still provide. Our initial results indicate that where the structures are very small (<1 mm) analysis is challenging because tiny vessel branches can look similar to pinpoint nodules.

In some initial studies both magnetic resonance and computed tomography imaging approaches were used, with magnetic resonance giving the better images due to its greater contrast between the hyperintense lesions and the hypointense, inflated lung parenchyma. Of the imaging options, T1-weighted magnetic resonance pulse sequence was the best due to its excellent lesion conspicuity. In a typical magnetic reso-

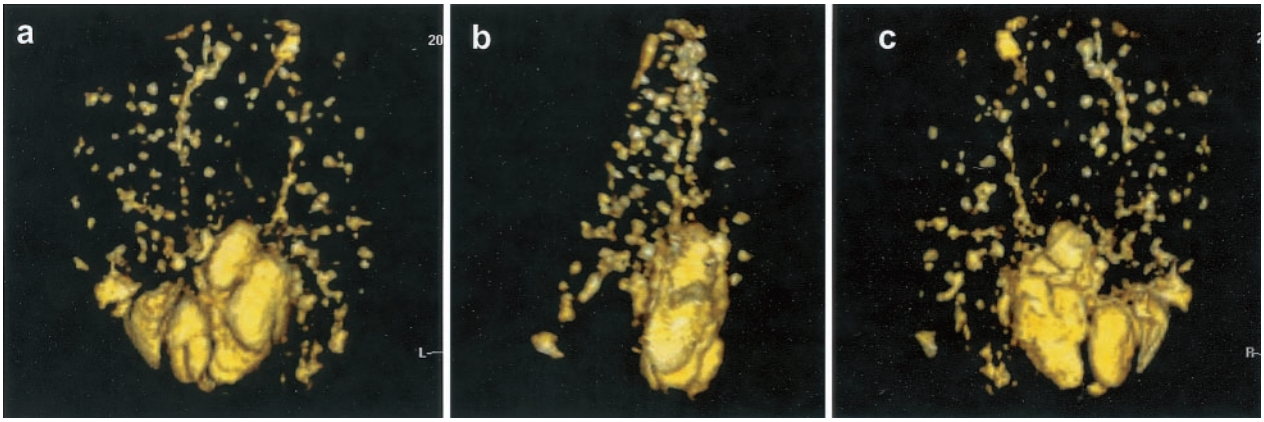

FIG. 4. Three-dimensional colorized reconstruction of a series of T1-weighted magnetic resonance images from a nonvaccinated control guinea pig thirty days after infection by aerosol with *M. tuberculosis*, showing anterior (a), lateral (b), and posterior (c) aspects. The large size of the enlarged cluster of lymph nodes is particularly noticeable. Linear structures extending into each lung lobe are pulmonary vessels.

nance experiment, 1.5-mm-thick sections generated 18 to 19 images that could then be used for three-dimensional reconstruction of the entire lung field.

Imaging technologies have proven useful for evaluating postmortem pathology, particularly brain specimens (7, 17, 20, 24, 27). Postmortem imaging allows assessment of lesion distribution and characterization and can be more sensitive than gross tissue examination (27). Although imaging studies can be relatively expensive, they can add important guidance for more detailed, accurate sampling and can provide a critical focus to pathological studies (20, 27). Magnetic resonance imaging of the lung specimens described here illustrates the distinct advantage that the entire lung field can be evaluated in a systematic uniform fashion, thus eliminating the sample bias that can occur by histopathologic analysis. Moreover, the imaging methods are completely nondestructive, preserving the tissue for further analysis.

To our knowledge, this is the first report on postmortem cross-sectional imaging of lung specimens in this type of model. An unexpected finding was that lung lesion nodules were most conspicuous on the T1-weighted magnetic resonance pulse sequence, since T2 and STIR pulse sequences are typically considered to have greater sensitivity than most forms of pathology because of their associated increased signal intensity from edema and cell infiltrate. The greater signal-to-noise ratio of T1-weighted images is a plausible explanation for the granulomas being more conspicuous by using that form of pulse sequence. As discussed above, the primary limitation in these initial studies was that the lesions in BCG-vaccinated animals were mostly quite small, but this technology has the potential ability to provide higher resolution images by adjusting imaging factors, by using custom-designed transmit-receive coils, or by using a scanner with a higher magnetic field strength.

Besides magnetic resonance imaging, a variety of other imaging modalities are gaining popularity for in vivo serial lesion detection in laboratory animals. These include radiography, computed tomography, ultrasound imaging, and bioluminescence imaging. Multiple factors and decisions are necessary to determine the best in vivo monitoring method for a particular research model. Each has its own unique advantages and dis-

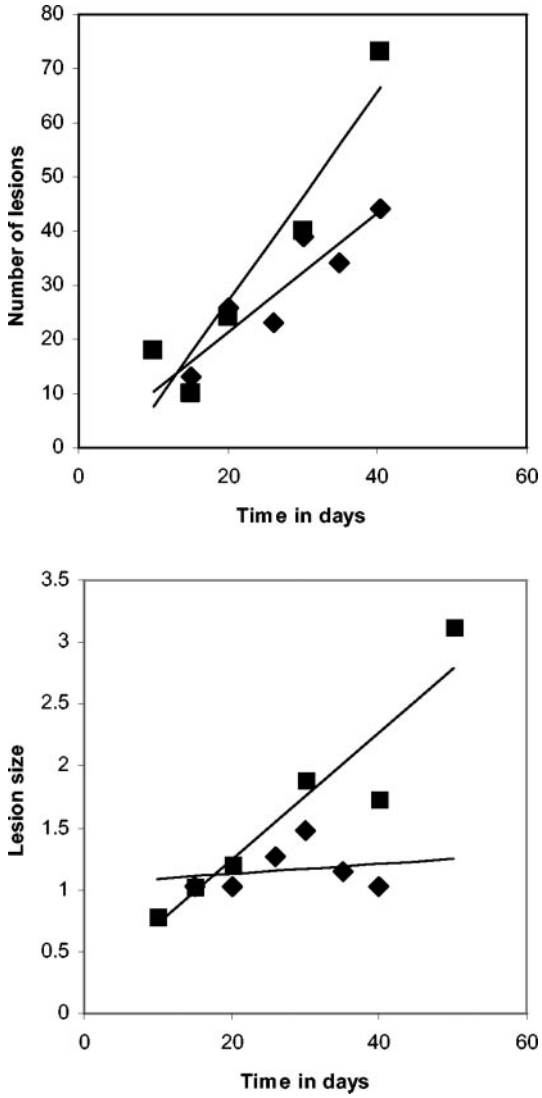

FIG. 5. Lesion numbers and sizes calculated from magnetic resonance images over the first 50 days of infection in individual nonvaccinated animals (■) and animals receiving BCG vaccination (♦). The lesion size datum scale is in cubic millimeters. Simple linear regression lines were calculated by using Microsoft Excel.

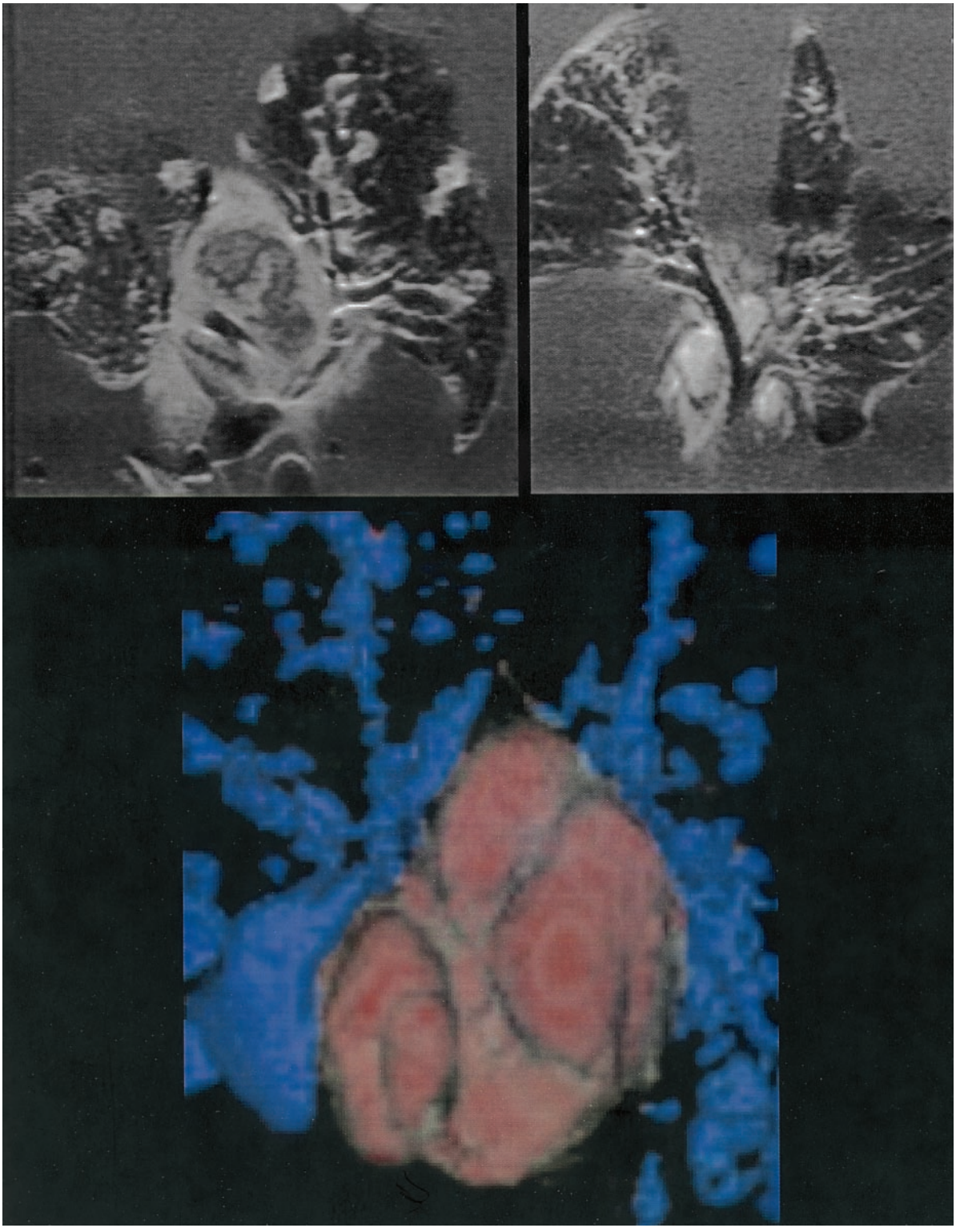

FIG. 6. Magnetic resonance images of lungs from a nonvaccinated guinea pig at day 30 of the infection (left) and a BCG-vaccinated animal (right). A large hyperintense perihilar lymph node is evident in the unprotected animal, with an irregular less intense center consistent with necrosis. In contrast, nodes in the vaccinated animals were small, oval, with no indication of necrosis. A colorized reconstructed image of the lymph node cluster in nonvaccinated animals is also shown (bottom panel).

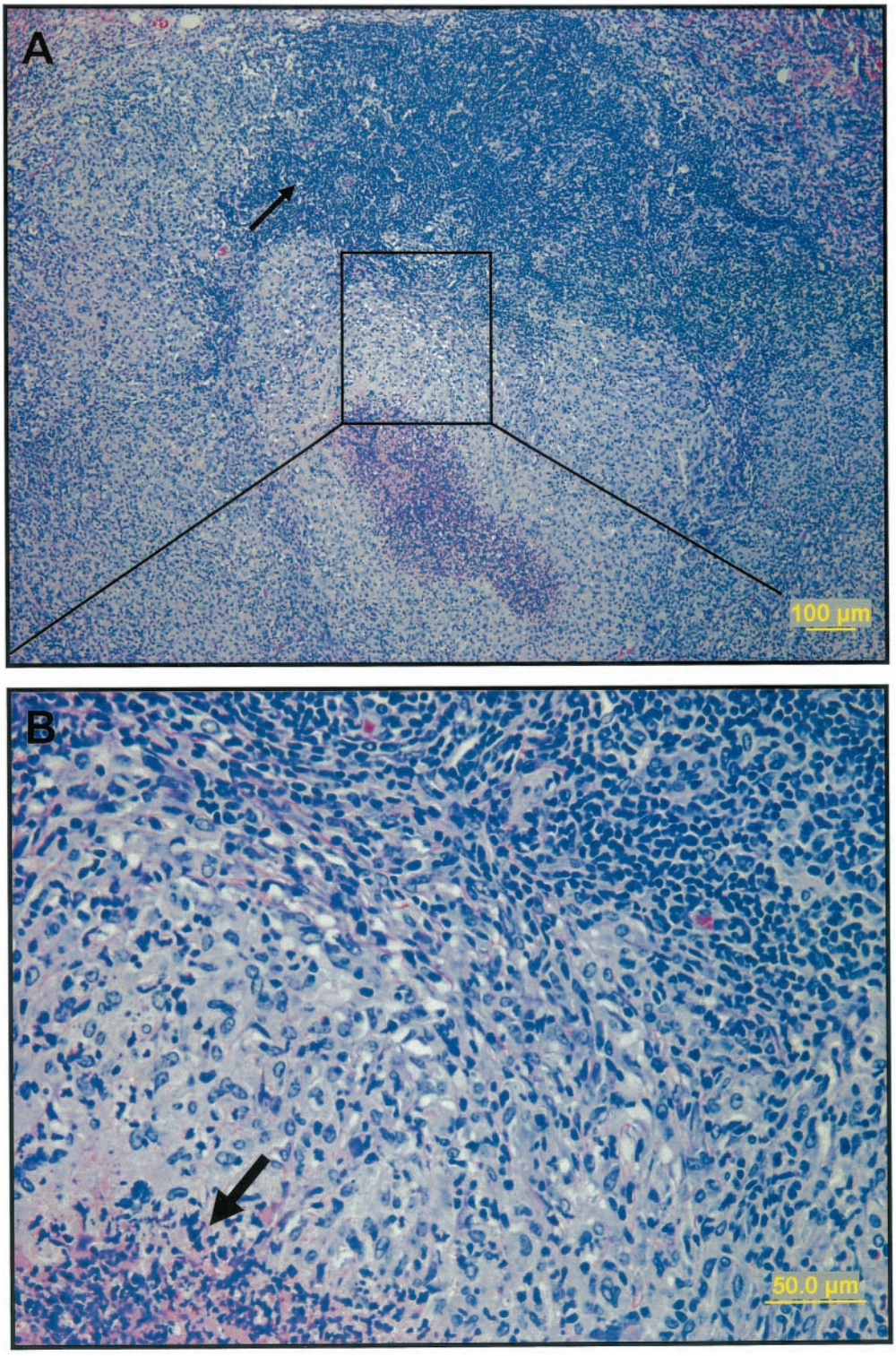

FIG. 7. Light photomicrographs of mediastinal lymph node from nonvaccinated guinea pig 30 days after exposure to aerosol infection. (A) There is extensive coalescing foci of granulomatous inflammation effacing the majority of the lymph node architecture, leaving a few remnants of mature lymphocytes (thin arrow). (B) A higher magnification of the area delineated by the rectangle in panel A shows predominantly epithelioid macrophages and fewer lymphocytes that surround foci of necrosis (thick arrow). Sections were stained with hematoxylin and eosin.

advantages that would need consideration depending upon the body region being evaluated and the type of lesion being detected. Practical factors include purchase price and operating cost of the modality, image quality, and oftentimes necessary tradeoffs between spatial resolution and sensitivity. Most imaging techniques rely on inherent biological properties for lesion detection or utilize injectable contrast media to improve sensitivity. Other techniques, such as bioluminescence, can be sensitive for imaging superficial lesions in vivo but require genetic manipulation to introduce a luciferase gene into the cell line of interest in order to get a functional bioluminescence reporter.

The approach described here may improve our understanding of the basic pathology of pulmonary tuberculosis in the guinea pig and ways in which prior vaccination may affect this process. At present, the general hypothesis is that inhalation of bacilli establishes primary lesions in the lungs (2, 16, 21, 23, 28). Because neither innate or the slowly emerging adaptive immune response can initially contain bacterial growth, some bacteria erode into adjacent blood vessels and escape (a process termed hematogenous dissemination). Some of these bacteria get trapped in the pulmonary vasculature (no one as yet has explained how), where they establish secondary lesions, which thrive in apical regions of the lungs (in the guinea pig, this would be the dorsal regions), where the relationship between the airflow and blood supply (i.e., the V/Q ratio) is most favorable to lesion reactivation (15).

Classical studies in the literature (10, 22, 29) have demonstrated that the effect of BCG is on the disease process rather than the initial infection. As a result, guinea pigs protected by BCG are thought to have similar numbers of lesions, but these lesions are much smaller. In the present study, we were able to observe and confirm these parameters directly. Lesion numbers in control animals and in vaccinated animals were much the same over the first 30 days of the infection. This increased later, indicating the establishment of secondary lesions. Moreover, the size of the lesions increased progressively in the control animals but remained relatively small in the vaccinated guinea pigs.

If the increased number of lesions in the controls after day 30 or so represent secondary lesions, then the magnetic resonance images indicate that these are also distributed relatively uniformly around the lungs, since we saw no evidence of any selective distribution to any one area of the lungs. As discussed above, it is thought that those established in V/Q-rich areas are the most likely to subsequently reactivate. As we have suggested elsewhere (26), when lesions reach a certain size they are likely to erode into large pulmonary vessels, facilitating this event.

The lesion number analysis also supports the hypothesis that a single bacillus establishes a single lesion, which is important information. These data are in stark contrast, however, to a recent study with a rabbit model, in which it was estimated that 300 to 1,800 bacilli are needed to establish lesions (13). It would be interesting to reevaluate the rabbit model by using the magnetic resonance technique described here.

The other important observation made in these studies was the severe lymphadenopathy seen in the mediastinal lymph node of unprotected animals. This has been extensively described before in the context of the bacterial burden in this lymph node cluster (22), and we show here that this can be seen both by imaging and by conventional histopathology. Indeed, by the latter approach we were able to observe the very extensive pathology and necrosis occurring in these tissues.

This, of course, establishes a paradox. The nodes appear to be seriously damaged very early in the disease process, and yet the animal at this point is strongly delayed-type hypersensitivity positive (15, 16) and is recruiting lymphocytes into granulomatous lesions in large numbers (26). It is currently believed that bacteria are carried from lung tissues to draining lymph nodes by dendritic macrophages, where they present antigens leading to T-cell sensitization driving the emergence of the acquired immune response (4, 8, 9). One would anticipate that this process would be severely disrupted in the guinea pig given the tissue damage and extensive necrosis in the lymph node, which would presumably limit and slow the emerging host response. The fact that it does not suggests that either sufficient lymphoid tissue remains intact during the early course of the infection or that bacteria and/or antigen is more widely dispersed throughout the immune system.

ACKNOWLEDGMENTS

This study was supported in part by the Merck-Merial Summer Research Fellowship Program and by National Institutes of Health grant AI054697.

We thank Billie Arceneaux and Melinda Wilhelm for outstanding technical support with the magnetic resonance imaging. Voxar, Ltd., Edinburgh, United Kingdom, provided the three-dimensional imaging software for this analysis.

REFERENCES

1. **Andersen, P.** 2001. TB vaccines: progress and problems. Trends Immunol. **22:**160–168.
2. **Balasubramanian, V., E. H. Wiegeshaus, B. T. Taylor, and D. W. Smith.** 1994. Pathogenesis of tuberculosis: pathway to apical localization. Tuberc. Lung Dis. **75:**168–178.
3. **Baldwin, S. L., C. D'Souza, A. D. Roberts, B. P. Kelly, A. A. Frank, M. A. Lui, J. B. Ulmer, K. Huygen, D. M. McMurray, and I. M. Orme.** 1998. Evaluation of new vaccines in the mouse and guinea pig model of tuberculosis. Infect. Immun. **66:**2951–2959.
4. **Bodnar, K. A., N. V. Serbina, and J. L. Flynn.** 2001. Fate of *Mycobacterium tuberculosis* within murine dendritic cells. Infect. Immun. **69:**800–809.
5. **Brandt, L., and I. Orme.** 2002. Prospects for new vaccines against tuberculosis. BioTechniques **33:**1098
6. **Britton, W. J., and U. Palendira.** 2003. Improving vaccines against tuberculosis. Immunol. Cell Biol. **81:**34–45.
7. **Bronge, L., N. Bogdanovic, and L. O. Wahlund.** 2002. Postmortem MRI and histopathology of white matter changes in Alzheimer brains: a quantitative, comparative study. Dement. Geriatr. Cogn. Disord. **13:**205–212.
8. **Gonzalez-Juarrero, M., and I. M. Orme.** 2001. Characterization of murine lung dendritic cells infected with *Mycobacterium tuberculosis*. Infect. Immun. **69:**1127–1133.
9. **Gonzalez-Juarrero, M., T. S. Shim, A. Kipnis, A. P. Junqueira-Kipnis, and I. M. Orme.** 2003. Dynamics of macrophage cell populations during murine pulmonary tuberculosis. J. Immunol. **171:**3128–3135.
10. **Ho, R. S., J. S. Fok, G. E. Harding, and D. W. Smith.** 1978. Host-parasite relationships in experimental airborne tuberculosis. VII. Fate of *Mycobacterium tuberculosis* in primary lung lesions and in primary lesion-free lung tissue infected as a result of bacillemia. J. Infect. Dis. **138:**237–241.
11. **Huygen, K.** 2003. On the use of DNA vaccines for the prophylaxis of mycobacterial diseases. Infect. Immun. **71:**1613–1621.
12. **Kaufmann, S. H.** 2000. Is the development of a new tuberculosis vaccine possible? Nat. Med. **6:**955–960.
13. **Manabe, Y. C., A. M. Dannenberg, Jr., S. K. Tyagi, C. L. Hatem, M. Yoder, S. C. Woolwine, B. C. Zook, M. L. Pitt, and W. R. Bishai.** 2003. Different strains of *Mycobacterium tuberculosis* cause various spectrums of disease in the rabbit model of tuberculosis. Infect. Immun. **71:**6004–6011.
14. **McMurray, D. N.** 2001. Determinants of vaccine-induced resistance in animal models of pulmonary tuberculosis. Scand. J. Infect. Dis. **33:**175–178.
15. **McMurray, D. N.** 2003. Hematogenous reseeding of the lung in low-dose, aerosol-infected guinea pigs: unique features of the host-pathogen interface in secondary tubercles. Tuberculosis **83:**131–134.

16. **McMurray, D. N., F. M. Collins, A. M. Dannenberg, Jr., and D. W. Smith.** 1996. Pathogenesis of experimental tuberculosis in animal models. Curr. Top. Microbiol. Immunol. **215:**157–179.
17. **Messori, A., and U. Salvolini.** 2003. Postmortem MRI as a useful tool for investigation of cerebral microbleeds. Stroke **34:**376–377.
18. **Orme, I. M.** 2001. The search for new vaccines against tuberculosis. J. Leukoc. Biol. **70:**1–10.
19. **Orme, I. M., D. N. McMurray, and J. T. Belisle.** 2001. Tuberculosis vaccine development: recent progress. Trends Microbiol. **9:**115–118.
20. **Shiga, T.** 1998. A comparative study of postmortem MR imaging and pathological examination of human brain specimens. Hokkaido J. Med. Sci. **73:** 497–504.
21. **Smith, D., E. Wiegeshaus, and V. Balasubramanian.** 2000. Animal models for experimental tuberculosis. Clin. Infect. Dis. **31**(Suppl. 3)**:**S68–S70.
22. **Smith, D. W., D. N. McMurray, E. H. Wiegeshaus, A. A. Grover, and G. E. Harding.** 1970. Host-parasite relationships in experimental airborne tuberculosis. IV. Early events in the course of infection in vaccinated and nonvaccinated guinea pigs. Am. Rev. Respir. Dis. **102:**937–949.
23. **Smith, D. W., and E. H. Wiegeshaus.** 1989. What animal models can teach us about the pathogenesis of tuberculosis in humans. Rev. Infect. Dis. **11**(Suppl. 2)**:**S385–S393.
24. **Thali, M. J., K. Yen, W. Schweitzer, P. Vock, C. Boesch, C. Ozdoba, G. Schroth, M. Ith, M. Sonnenschein, T. Doernhoefer, E. Scheurer, T. Plattner, and R. Dirnhofer.** 2003. Virtopsy, a new imaging horizon in forensic pathology: virtual autopsy by postmortem multislice computed tomography (MSCT) and magnetic resonance imaging (MRI): a feasibility study. J. Forensic Sci. **48:**386–403.
25. **Turner, O. C., R. J. Basaraba, A. A. Frank, and I. M. Orme.** 2003. Granuloma formation in mouse and guinea pig models of experimental tuberculosis, p. 65–84. *In* D. L. Boros (ed.), Granulomatous infections and inflammations: cellular and molecular mechanisms. ASM Press, Washington, D.C.
26. **Turner, O. C., R. J. Basaraba, and I. M. Orme.** 2003. Immunopathogenesis of pulmonary granulomas in the guinea pig after infection with *Mycobacterium tuberculosis*. Infect. Immun. **71:**864–871.
27. **van den Hauwe, L., P. M. Parizel, J. J. Martin, P. Cras, P. De Deyn, and A. M. De Schepper.** 1995. Postmortem MRI of the brain with neuropathological correlation. Neuroradiology **37:**343–349.
28. **Wiegeshaus, E., V. Balasubramanian, and D. W. Smith.** 1989. Immunity to tuberculosis from the perspective of pathogenesis. Infect. Immun. **57:**3671–3676.
29. **Wiegeshaus, E. H., D. N. McMurray, A. A. Grover, G. E. Harding, and D. W. Smith.** 1970. Host-parasite relationships in experimental airborne tuberculosis. 3. Relevance of microbial enumeration to acquired resistance in guinea pigs. Am. Rev. Respir. Dis. **102:**422–429.

Editor: S. H. E. Kaufmann